Article

Multi-Level Numerical Modelling and Analysis of Tile Vaults

David López López [1,*], Nuno Mendes [2], Daniel V. Oliveira [2], Lucrecia J. Calderón Valdiviezo [1] and Marta Domènech-Rodríguez [3]

1   Department of Architectural Technology, Universitat Politècnica de Catalunya, 08028 Barcelona, Spain; lucrecia.calderon@upc.edu
2   Department of Civil Engineering, Institute for Sustainability and Innovation in Structural Engineering (ISISE), Advanced Production and Intelligent Systems (ARISE), University of Minho, 4800-058 Guimarães, Portugal; nunomendes@civil.uminho.pt (N.M.); danvco@civil.uminho.pt (D.V.O.)
3   Department of Architectural Design, Universitat Politècnica de Catalunya, 08028 Barcelona, Spain; marta.domenech@upc.edu
*   Correspondence: david.lopez.lopez@upc.edu

Abstract: The complex structural behaviour of masonry, with its brittle response in tension, frictional response in shear, and anisotropy, makes it challenging to model accurately. Tile vaults, with their unique features such as different binders and bricks placed flat, have distinctive structural performance, and determining the most suitable assessment method is still a subject of debate in both academic and professional circles. This paper presents a study on the structural analysis of tile vaults, aiming at evaluating different numerical approaches for this type of structure. The examination of these approaches and their effectiveness in capturing the structural behaviour of tile vaults intends to offer valuable insights to researchers and professionals in this field. Experimental research was initially carried out in order to provide data for the calibration of the structural models. Two full-scale vaults were tested. Furthermore, several material characterization tests were also performed. The numerical assessment was carried out through limit analysis and non-linear static analysis with numerical models based on the Finite Element Method (FEM). Two FEM models were prepared using different modelling approaches for masonry, namely the macro-modelling and the simplified micro-modelling approaches. The results of the limit analysis presented a load capacity significantly lower than the ultimate load obtained from the experimental tests. The calibrated FEM models presented good results in comparison to the experimental results, namely in terms of damage pattern and load capacity.

Keywords: tile vault; Catalan vault; experimental test; FEM; limit analysis; masonry

1. Introduction

Tile, thin-tile, Catalan, timbrel or Guastavino vaulting is a traditional construction technique to build masonry structures. Vaults and shells can be built without any formwork thanks to the use of light bricks (either tiles or hollow bricks) and a fast-setting binder for the first layer, which serves then as formwork for the subsequent brick courses [1]. This construction scheme together with the availability and affordability of the materials involved made up the appropriate combination to create a traditional building system in the area close to the Spanish Mediterranean coast, which was afterwards spread to different parts of the world.

Some authors have identified a possible precedent in a similar construction technique by the Romans [2], who used ceramic pieces as stay-in-place formwork for their particular concrete [3], while other researchers observe a later clear origin either in the north-east [4,5] or south-east of Spain [6].

The "Catalan" adjective for the tile vaults has its origin in the technique's peak in terms of expressiveness and versatility during the Catalan Modernism period, thanks to the works of Antoni Gaudí Cornet and Lluís Domènech i Montaner, among others [7]. The

"Guastavino" adjective comes from the Spanish architects (father and son) with that surname who emigrated to the United States in 1881 and built there hundreds of extraordinary, innovative timbrel vaults [8]. The study of the tile vaults existing in Cuba has also been the object of recent research [9–13].

The current environmental crisis urges the construction of more sustainable structures, necessitating a radical shift in our contemporary design and building practices [14]. In response to this imperative, the recovery and integration of traditional construction techniques emerge as a promising approach. By leveraging local and sustainable materials, these age-old methods offer potential solutions to mitigate the adverse impacts of construction on the environment [15–17].

To effectively harness the benefits of traditional construction techniques, it is imperative to adapt and modernize them to align with present-day demands and challenges [18–25]. A comprehensive understanding of their construction processes and structural behaviour is crucial to ensure their seamless integration into contemporary building practices. Additionally, there is a pressing need for innovative advancements aimed at reducing their carbon footprint and enhancing their economic viability [26].

Projects featuring tile vaults are currently spreading around the world, boosted by architects and engineers who envisaged opportunities related to economy, aesthetics and the sustainability of this construction technique [27]. Cutting-edge, form-finding and structural analysis computational tools are being used to safely shape these masonry structures and create unique contemporary architectural pieces [28–31]. Furthermore, research on the combination of tile vaulting with reinforcement and/or concrete has also been carried out [32–34], exploring new construction techniques to build, for instance, economic, composite (masonry and reinforced concrete) shells [35–37], or geogrid-reinforced, soil tile vaults [38]. Textile reinforced mortar has also been used to strengthen tile vaults [39,40], as well as a glass-fibre-reinforced polymer mesh [41–43].

Limit analysis [44] has been traditionally used for the safety assessment of masonry vaults, focusing on determining the collapse mechanism and force capacity. Both static and kinematic approaches (i.e., lower-bound [45–50] and upper-bound [51–54] theorems, respectively) are a matter of research. However, when there is a specific interest in understanding displacement capacity and damage evolution, researchers often turn to continuum approaches [55–59] or discrete approaches [60–63]. Due to the masonry's composite character, namely its brittle response in tension, frictional response in shear and anisotropy, its complex structural behaviour is today still difficult to model [64].

The specific features of tile vaults, involving different binders and placing the bricks flat (with the bed of the first course of tiles defining the intrados), confer unique structural performance on this construction technique, whose most appropriate assessment method is still a matter of discussion both in the related academic and professional domains [65]. The use of accurate models and non-conservative safety factors becomes particularly important when dealing with the restoration of existing constructions, whose usual high slenderness is, in many cases, challenging to the assessing architect or engineer. An inappropriate structural evaluation of constructions may result in their demolition, which is unfortunately not uncommon among professionals working in the field, mainly due to the use of erroneous material properties and linear elastic approaches. It is noted that the linear elastic FE analysis is not adequate to assess the structural performance of existing masonry constructions [64,66].

This paper presents research on the structural analysis of tile vaults, aiming to contribute to a better understanding of their behaviour and to determine the most appropriate numerical modelling approaches for the analysis of tile vaults. The combination of experimental and numerical analysis is strongly advisable when addressing the analysis of masonry structures to obtain the data for the numerical models and validate the numerical results. This approach was followed in the present study.

Experimental tests on specimens were performed, aiming at obtaining the physical and mechanical properties of the materials. Furthermore, tests on full-scale vaults were also

carried out. The collected data was processed to validate the numerical model of the vault adopted for this study. Two structural analysis techniques were used, namely: (a) limit analysis; (b) non-linear static analysis. The non-linear static analysis was carried out using a numerical model based on the FEM and for two numerical modelling approaches [67], namely, (a) macro-modelling approach, in which units, mortar and unit/mortar interface are smeared out in a homogeneous continuum material; and (b) simplified micro-modelling approach, in which the expanded units are represented by continuum elements, whereas the behaviour of the mortar joints and unit/mortar interface is lumped in discontinuous elements.

2. Experimental Tests and Generated Data

2.1. Material Properties

Several experimental tests on specimens and full-scale vaults were carried out at the Laboratory of Materials and Quality Control of the School of Building Construction at the Polytechnical University of Catalonia (UPC), aimed at obtaining the material properties needed for the numerical analysis and the experimental response (maximum load capacity and deformation) of the structure. When the specifications provided by the manufacturer and the recommendations present in the literature provided reliable data on the material properties, those were taken into account and no tests were performed.

The construction of vaults involved three materials, namely bricks, gypsum and mortar. The vaults were made of hollow bricks of 28 cm $\times$ 14 cm $\times$ 4 cm with a volume equal to 1.57×10^{-3} m^3. Each brick weighs 1.5 kg and the density (ρ) is equal to 954.7 kg/m^3. A fast-setting gypsum was used to build the first course of bricks, "Iberplast B1" [68], with a water/gypsum (L/kg) ratio of 0.66, complying with UNE-EN 13.279-1:2006 [69]. A grey dry Portland cement mortar M7.5 was the binder used to build the second course of bricks. A water/dry mortar (L/kg) ratio of 0.17 was adopted.

For the macro-modelling approach, several parameters of the materials are needed, namely: (a) density (ρ) (also needed for the limit analysis); (b) Young's modulus (E); (c) Poisson's ratio (ν); (d) compressive strength (f_c); (e) compressive fracture energy (G_{fc}); (f) tensile strength (f_t); and (g) tensile fracture energy (G_{fl}). Four flat specimens of the vault were built, see Figure 1. The specimens' volume is 1.99×10^{-2} m^3, with dimensions of 0.475 m $\times$ 0.475 m $\times$ 0.088 m. They have an average weight of 24.21 kg and a density of 1219.4 kg/m^3. The Young's modulus (E) of the masonry, equal to 3118 N/mm^2, and the compressive strength (f_c), equal to 5.90 N/mm^2, were obtained through compression tests on specimens. The compressive fracture energy (G_{fc}) can be calculated from Equation (1):

$$G_{fc} = d \cdot f_c \tag{1}$$

where a value d (ductility index) equal to 1.6 mm is recommended for $f_c < 12$ N/mm^2 [70]. The Poisson ratio (ν) was defined according to typical values for masonry present in the literature (0.15) [67]. The tensile strength and the tensile fracture energy (G_{fl}) were the parameters used to calibrate the model. An initial value of 5% of the compressive strength (0.295 N/mm^2) for the tensile strength and a value equal to 0.012 N/mm [67] for the tensile fracture energy were adopted. The shear behaviour was assumed as a linear relationship between principal stresses and strains, in which the shear stiffness is reduced after cracking to 0.10 of its initial value. The adopted material properties, after the numerical calibration, for the macro-model are presented in Table 1.

Table 1. Material properties for the macro-model.

Young's Modulus	Poisson's Ratio	Density	Tension		Compression	
E	ν	ρ	f_t	G_{ft}	f_c	G_{fc}
N/mm^2	-	kg/m^3	N/mm^2	N/mm	N/mm^2	N/mm
3200	0.15	1219.4	0.24	0.14	5.90	9.44

**Figure 1.** Compression test on vault specimens.

In what concerns the preparation of the simplified micro-model, tile vaults present some challenges for the assessment of structural performance using this approach. One of them is related to the different orientation of bricks in each course (see Figure 2), as the bricks do not have the same mechanical properties for each direction.

Figure 2. Construction of the vault: (**left**) first layer; and (**right**) second layer.

In the simplified micro-modelling approach, the brick units were considered linear elastic elements. Thus, only the interfaces present non-linear behaviour. The linear properties of the interfaces and units and the non-linear properties of the three interface types (to be listed later) are needed, see also Figure 3. The linear properties of the interfaces and units are (a) Poisson's ratio (ν) and Young's modulus (E) of the brick in its vertical and horizontal directions (Figure 2); and (b) normal and shear stiffness (k_n and k_s) of the three interfaces, for which the Young's and shear moduli (E and G) of binders and bricks in the three directions

are needed. The non-linear properties of the interfaces are (a) tensile strength (f_t); (b) tensile fracture energy (G_{fI}); (c) cohesion (c); (d) friction and dilatancy angles (*tanφ* and *tanφ*); (e) shear fracture energy (G_{fII}); (f) compressive strength (f_c); (g) compressive fracture energy (G_{fc}); and (h) equivalent plastic relative displacement (k_p).
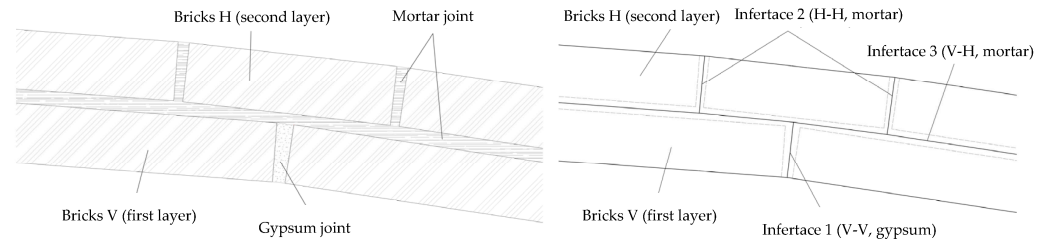
Figure 3. Two-layer tile vault: (**left**) arrangement of the masonry; and (**right**) units and interfaces of the simplified micro-model ("V" and "H" correspond to the vertical and horizontal direction of the units, respectively).

The Young's modulus and the compressive strength of the bricks in the vertical direction were obtained by testing four brick specimens. The average of Young's modulus and compressive strength of four specimens in the vertical direction is equal to 7748 N/mm² and 21.04 N/mm², respectively. In the other two directions, Young's moduli equal to 5936 N/mm² and 2665 N/mm² were obtained for the horizontal and orthogonal directions, respectively.

According to the characteristics of construction, the vault presents three types of interfaces (Figure 3, right), namely (a) interface 1, made with gypsum between bricks in the vertical direction; (b) interface 2, made with mortar between bricks in the horizontal direction; and (c) interface 3, between the two layers, made with mortar between bricks in the vertical and horizontal directions.

Young's moduli of mortar and gypsum, and the Poisson's ratio of bricks were obtained from the literature [71] and the technical specifications defined by the manufacturer. The shear modulus (G) was computed using Equation (2):

$$G = \frac{E}{2 \cdot (1 + \nu)}. \tag{2}$$

The normal and shear stiffness of interfaces were calculated by applying the following equations [66]:

$$k_n = \frac{E_u \cdot E_m}{h_m \cdot (E_u - E_m)}, \tag{3}$$

$$k_s = \frac{G_u \cdot G_m}{h_m \cdot (G_u - G_m)}. \tag{4}$$

in which E_u and E_m are the Young's moduli of the units and the mortar/gypsum, respectively; G_u and G_m are the shear moduli of the unit and the binder, respectively; and h_m is the joint thickness. The joints present an average thickness of 8 mm.

Twelve specimens of gypsum were tested in compression according to EN 1015 [72]. The load was applied through an area of 40 mm × 40 mm. The average compressive strength is equal to 19.56 N/mm². The compressive strength of the mortar (7.5 N/mm²) was obtained from the technical specifications defined by the manufacturer (grey dry mortar 7.5). The compressive fracture energy was derived from two different equations as a function of f_c [71]:

$$G_{fc} = 15 + 0.43\, f_c - 0.0036\, f_c^2 \text{ (N/mm); for } 12\,\text{N/mm}^2 < f_c < 80\,\text{N/mm}^2, \tag{5}$$

$$G_{fc} = d \cdot f_c; \text{ for } f_c < 12\,\text{N/mm}^2 \text{ a } d = 1.6\,\text{mm is recommended.} \tag{6}$$

The values of *tanφ*, *tanφ*, G_{fII} and k_p were assumed according to the literature. The cohesion, c, was estimated as $1.5f_t$ [71]. As assumed for the macro-model, the tensile

strength and tensile fracture energy of the micro-model are defined as the parameters to calibrate. The material properties adopted for the micro-model are presented in Tables 2–4.

Table 2. Young and shear moduli of the materials.

	E N/mm^2	G N/mm^2
Bricks V	7750	3370
Bricks H	6000	2609
Mortar	1800	783
Gypsum	100	43
Bricks V-H	2700	1174

Table 3. Linear properties of the interfaces and units.

Element	Young's Modulus E N/mm^2	Poisson's Ratio ν -	Normal Stiffness k_n N/mm^3	Shear Stiffness k_s N/mm^3
Bricks V (first layer)	7750	0.15	-	-
Bricks H (second layer)	6000	0.15	-	-
Interface 1 (V-V, gypsum)	-	-	13	6
Interface 2 (H-H, mortar)	-	-	321	140
Interface 3 (V-H, mortar)	-	-	675	293

Table 4. Non-linear properties of the interfaces.

Element	Tension			Shear			Compression		
	f_t N/mm^2	G_{fI} N/mm	c N/mm^2	$tan\phi$ -	$tan\varphi$ -	G_{fII} N/mm	f_c N/mm^2	G_{fc} N/mm	k_p N/mm^2
Interface 1	0.80	0.14	1.20	0.75	0	0.093	19.56	22.03	10
Interface 2	0.32	0.14	0.48	0.75	0	0.093	7.50	12.00	10
Interface 3	0.32	0.14	0.48	0.75	0	0.093	7.50	12.00	10

2.2. Load Tests of Vaults

The vault adopted for this study presents the usual dimensions and characteristics of tile vaults traditionally used in dwellings. The vault adopted for this study (Figure 4) is a 1 m wide, 0.3 m high and 3 m span barrel vault composed of two layers of hollow bricks (88 mm thick in total).

Two layers of bricks

0.30 m

3.00 m
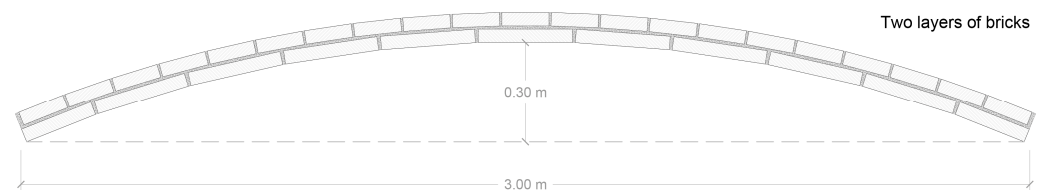
Figure 4. Cross-section of the vault.

Two vaults were built and tested, applying a load at $\frac{1}{4}$ of the vault's length on a platform constructed to create a flat surface 0.4 m wide and 1.0 m long (vault's width) (Figures 5 and 6). The setup included two metallic beams at the supports with two tie rods installed to absorb the horizontal thrust (Figure 5).

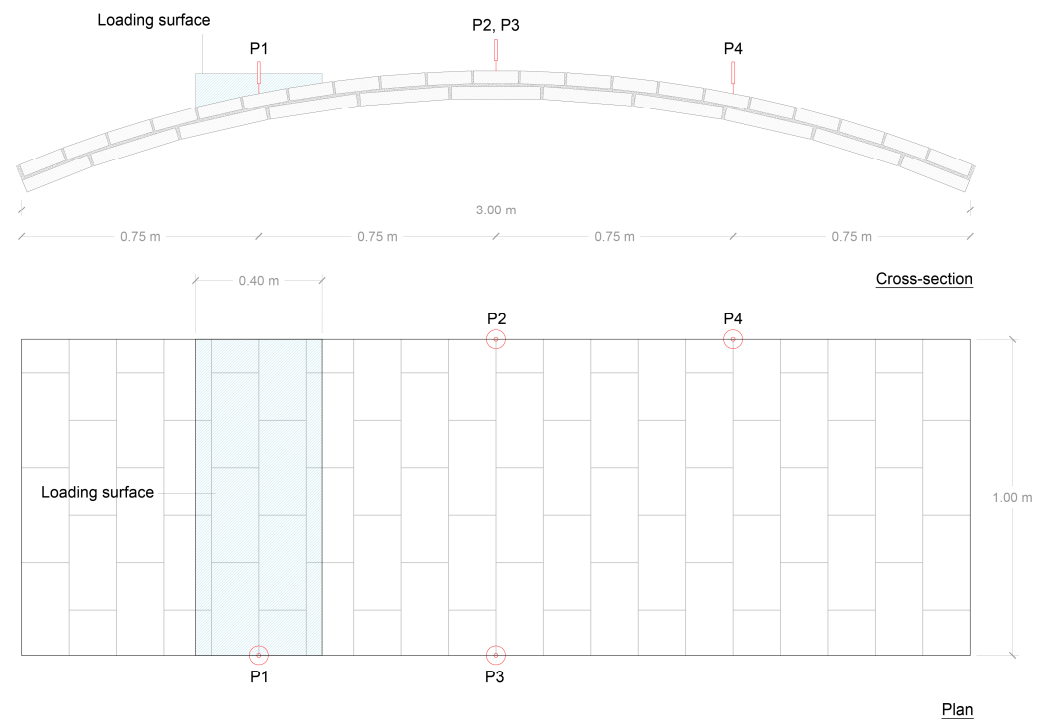**Figure 5.** Preparation of the load test.

Figure 6. First vault's potentiometers' distribution.

Four potentiometers were installed on the first vault, aimed at monitoring the displacements (Figure 6). The average values of the data registered by the potentiometers at the vault's edges, P2 and P3 (Figure 6), are called P2-P3 and estimate the displacements in the central point of the vault, both regarding the width and the length. The potentiometers in the P1 and P4 positions supply data concerning the vault's edges' displacements at the spots indicated in Figure 6. A torsion phenomenon can be identified, as the values from P2 are positive, whereas those from P3 are negative, meaning that one edge is subjected to downward displacements while the opposite one is subjected to upward displacements. An identical behaviour across the entire width of the vault was not expected due to imperfections caused by the manual construction process and potential small asymmetries in the loading process.

As awaited, the loaded side of the vault presents a downward displacement (positive) (P1), whereas the potentiometer at the opposite side (P4) registered negative values (Figure 7). P2–P3 data also indicate upward displacements, but very slight ones. For this

type of loading, the displacement at midspan is very low and generally not regarded as a reference point. Minor irregularities in the vault's shape can result in slight variations in the displacements at the central point (often hovering around zero), potentially altering their direction.
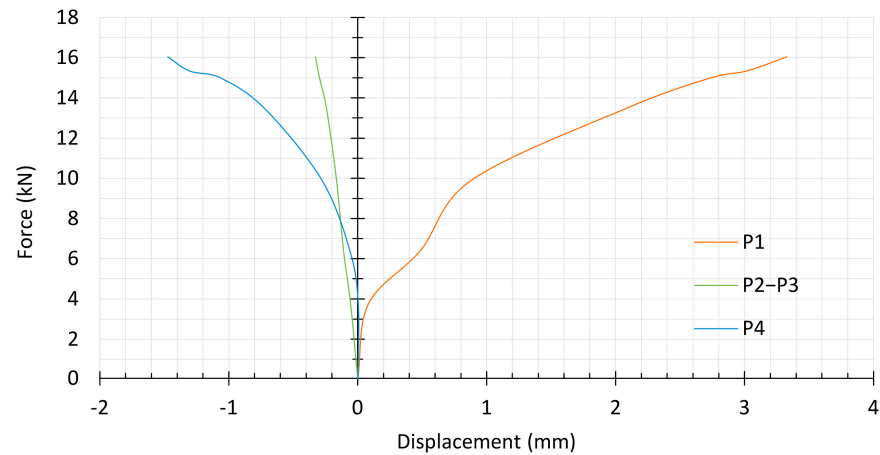
Figure 7. Load-displacement curves of the first vault's test.

The ultimate load reached 16.0 kN and no cracks were visible until the collapse. The collapse occurred suddenly, which is associated with unreinforced masonry's brittle behaviour. Taking into account the shape of the vault and the load's point of application, a four-hinge mechanism was expected to be developed during the loading test [44]. This behaviour was indeed observed in the vault, and the presence of the four-hinge mechanism could be inferred after collapse from the broken parts of the vault (Figure 8).

Figure 8. First vault collapsed. Red arrows show the identified hinges.

Four potentiometers were also used to monitor the displacements of the second vault (Figures 9 and 10). However, in this test, the potentiometers were placed in a distribution designed to obtain the displacements of three points at the central section directly. The distribution of the four potentiometers is presented in Figure 10. The displacement at the load point, called P1-P2, is taken as the average between the data registered by potentiometers P1 and P2. The displacements until the load of 12.5 kN were not properly measured by the potentiometers due to a technical limitation; these data are therefore not presented and only the displacements after that load are reported.

Figure 9. Load test on the second vault.
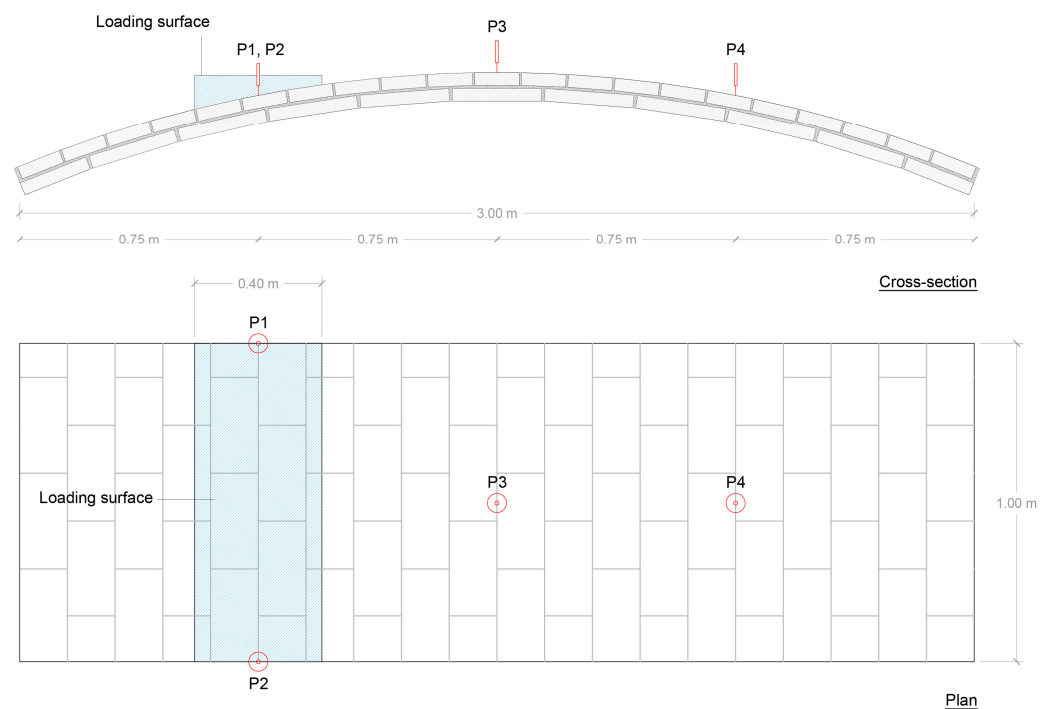
Figure 10. Second vault's potentiometers' distribution.

The ultimate load was equal to 13.19 kN and, as observed in the first vault, the failure mechanism involved four hinges (Figure 11, left). The displacements at 13.19 kN were 4.45 mm and 0.06 mm downwards for P1-P2 and P3, respectively, and 4.05 mm upwards for P4 (Figure 10). During this test, it was possible to observe a crack for a load equal to 12.5 kN. The crack was located on a single brick under the load at the edge of the vault (Figure 11, right).

Figure 11. Load test on the second vault: (**left**) end of testing with red arrows showing the identified hinges; and (**right**) crack during the load test (12.5 kN).

3. Modelling of the Structural Performance of the Vault

The numerical modelling of the structural performance of the vault was carried out based on two different methods, namely the limit analysis and non-linear static analysis. As mentioned above, two numerical models based on the Finite Element Method (FEM) were employed for the non-linear static analysis. The FEM models were prepared based on different modelling approaches for masonry, namely the macro-modelling approach, in which units, mortar and the unit/mortar interface are smeared out as a homogeneous continuum material, and the simplified micro-modelling, in which the expanded units are represented by continuum elements, whereas the behaviour of the mortar joints and unit/mortar interface is lumped in discontinuous elements [73].

3.1. Limit Analysis

In the limit analysis, the lower bound theorem (static approach), the upper bound theorem (kinematic approach) and the uniqueness theorem were adopted [74]. The vault was divided into 46 voussoirs and a density equal to 12.19 kN/m^3, obtained from the experimental tests, was used for the masonry. Each voussoir presents a volume of 0.006 m^3, which corresponds to a weight of 0.073 kN. The incremental load was applied over a length of 0.40 m to replicate the experimental test. The software ELARM, Extended Limit Analysis for Reinforced Masonry, was used to perform this assessment [36,75].

The ultimate load obtained from the limit analysis was equal to 3.84 kN (Figure 12), which is not similar to the ultimate load obtained from the experimental tests. According to this analysis, the load capacity of the vault is lower than one-third of the minimum collapse load obtained from the two experimental tests. Thus, the limit analysis seems conservative to evaluate the load capacity of these vaults. It is noted that limit analysis assumes the hypothesis that the masonry has no tensile strength along the voussoir interfaces [44], which is a cause for the low ultimate load obtained.
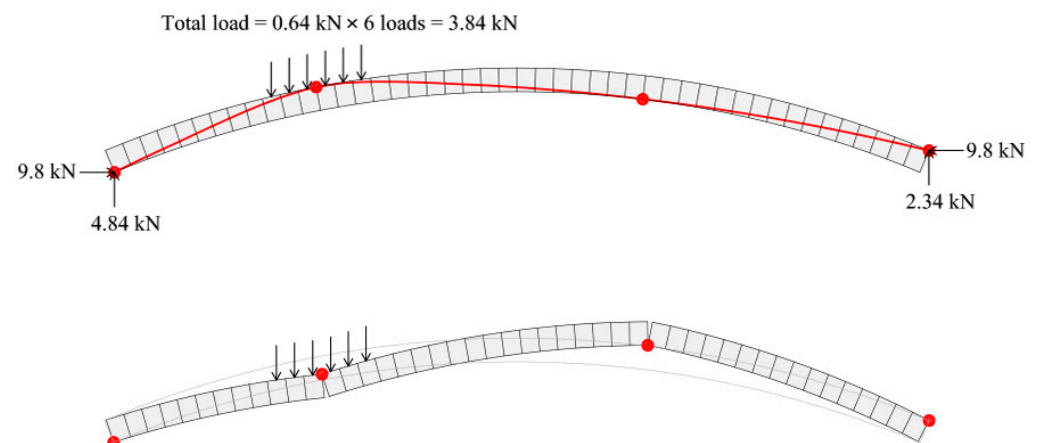
Figure 12. Limit analysis: (**top**) vault divided into 46 voussoirs; and (**bottom**) uniqueness theorem.

3.2. Macro-Modelling Approach

The software DIANA FEA was used to carry out this analysis. In the non-linear static analysis based on the macro-modelling approach, the Total-Strain Fixed-Crack Model, which corresponds to a model based on total strains, was selected due to its robustness and simplicity. It assumes that the cracks are fixed according to the principal directions of the strains and remain invariant during the loading of the structure. Quadrilateral isoparametric plane stress elements with eight nodes (CQ16M) based on quadratic interpolation and Gauss integration were used [76]. A mesh with a size of 38×22 mm was adopted.

In what concerns the stress–strains relationships, a parabolic hardening and softening curve for the compressive behaviour and exponential tension-softening for the tensile behaviour were adopted. The shear behaviour was simulated by a linear relationship between stress and strains, in which the shear stiffness is reduced after cracking according to the shear retention factor (0.1) [76].

The boundary conditions of the vaults in the experimental tests are complex and do not correspond to pinned (translations) or fixed (translations and rotations) supports. The observation of the damage, namely the position of the hinges, can be helpful for defining the boundary conditions of the numerical model. If the hinges in any of the two vaults are not located at the supports, but inside the vault, it means that the supports should be fixed. In this case study, both cases were found (Figure 13) and the two types of boundary conditions were evaluated. For the different boundary conditions, the tensile strength (f_t) and tensile fracture energy (G_{fl}) were calibrated. The other material properties were assumed as fixed parameters and were obtained from the experimental tests and data collection (Section 2). For the numerical model with pinned boundary conditions, the calibrated tensile strength is almost 14% of the compressive strength, which is a ratio considerably higher than those found in the literature [66,71,74]. The tensile strength and the tensile fracture energy obtained for the model with fixed boundary conditions are equal to 0.24 N/mm^2 and 0.14 N/mm, respectively, which are more appropriate for masonry. Thus, the numerical model with fixed boundary conditions was adopted for the assessment of the vault.


Figure 13. Details of the damage at the supports: (**left**) hinge before the support; and (**right**) hinge at the support.

The material properties used for the non-linear analysis are presented in Table 1. First, the self-weight was applied and then an overload over a length of 0.40 m was applied at one quarter of the span of the vault until failure. The capacity curves for the two control points (P1 and P4 for the first vault and P1-P2 and P4 for the second one) are presented in Figure 14. It is noted that the displacements of the capacity curves of the first vault were obtained from the edges of the vault (Figure 6). Due to the torsion effect (Section 2.2), these displacements are not equal to the displacements at the central section of the vault. Observing the direction of the displacements in each point and the torsion effect, it can be concluded that in the case of the loaded side, the central point's downward displacement is bigger than that on the edge. On the opposite side, the central point's upward displacement is bigger than

that on the edge. This is also in agreement with the curves of the first vault tested, which show less displacement in both graphics (Figure 14). In what concerns the load capacity of the vault, the numerical model presents a maximum load of 14.35 kN, which is within the results range obtained in the two experimental tests. Finally, the numerical model is able to simulate the damage observed in the experimental tests, in which the typical four hinges are observed (Figure 15).
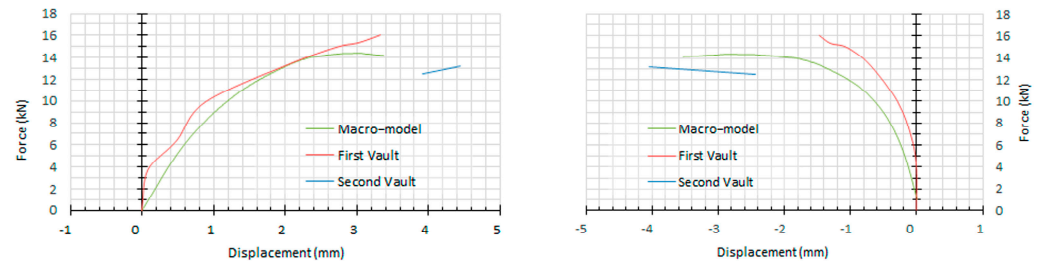

Figure 14. Numerical (macro-model) and experimental load-displacement curves: (**left**) response at the load point; and (**right**) response at the opposite side of the loading. (For the second vault, only the displacement after the load of 12.5 kN is shown).
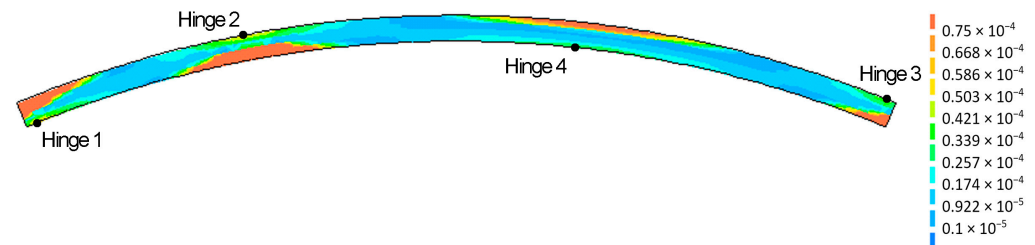
Figure 15. Principal tensile strains and hinges of the macro-model.

3.3. Simplified Micro-Modelling Approach

In the simplified micro-model, the elements utilized for the units are identical to those used for the macro-modelling approach: quadrilateral isoparametric plane stress elements with eight nodes, called "CQ16M" in the software DIANA FEA. A mesh of smaller finite elements is required to fit them within the dimensions of the bricks in both directions. The finite elements have a size of 19×22 mm. The interface elements are modelled as inelastic and had zero thickness and six nodes based on quadratic interpolation [76]. The yield surface adopted for the interface elements is defined by the function presented in Figure 16, where f_m is the compressive strength, f_t is the tensile strength, t_t is the shear traction, t_n is the normal traction and c is the cohesion. The diagrams of the behaviour of the model in compression, tension and shear are presented in Figure 17.
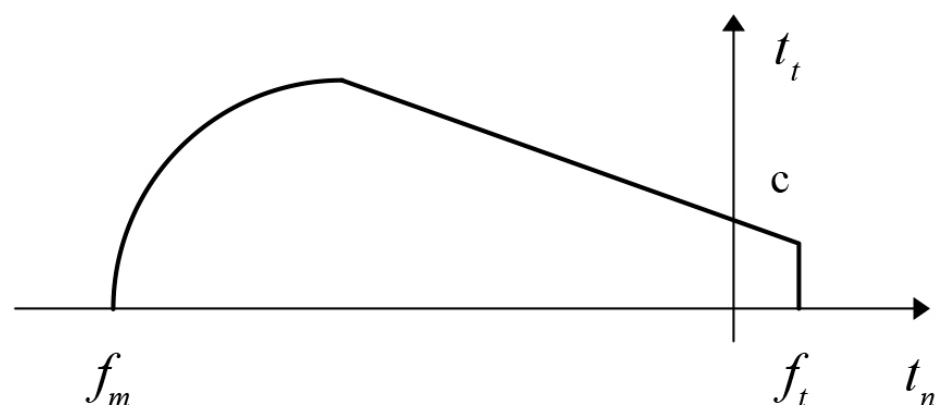

**Figure 16.** Yield surface of the interface elements [76].
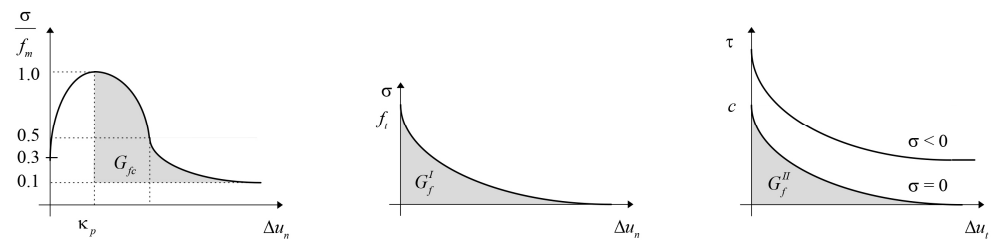
Figure 17. Material behaviour of masonry for the simplified micro-model: (**left**) compressive behaviour; (**middle**) tensile behaviour; and (**right**) shear behaviour [76].

The simplified micro-model was calibrated using the same procedure adopted for the macro-model. Thus, different boundary conditions were evaluated and it was concluded that the model with fixed boundary conditions presents results more in accordance with both the experimental tests and the literature [67,73,74].

Figure 18 presents the load-displacement curves for the two control points of the simplified micro-model and those from the experimental tests. The simplified micro-model presents a collapse mechanism with four hinges (Figure 19), which is in agreement with the damage observed in the experimental tests.
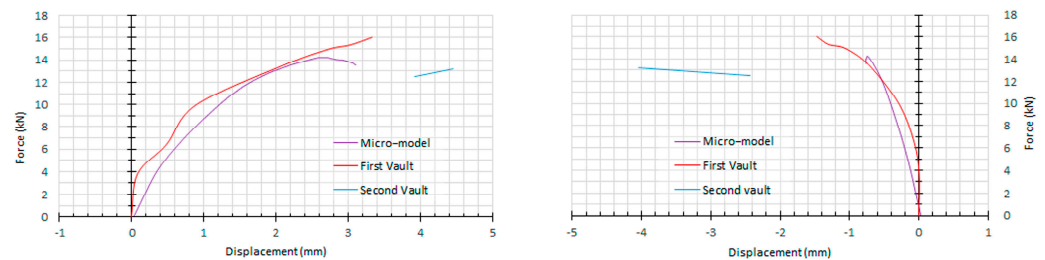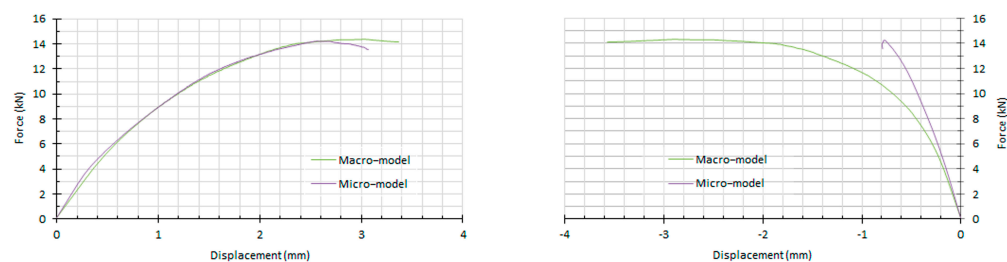

Figure 18. Numerical (simplified micro-model) and experimental load-displacement curves: (**left**) response at the load point; and (**right**) response at the opposite side point. (For the second vault, only the displacement after the load 12.5 kN is shown).
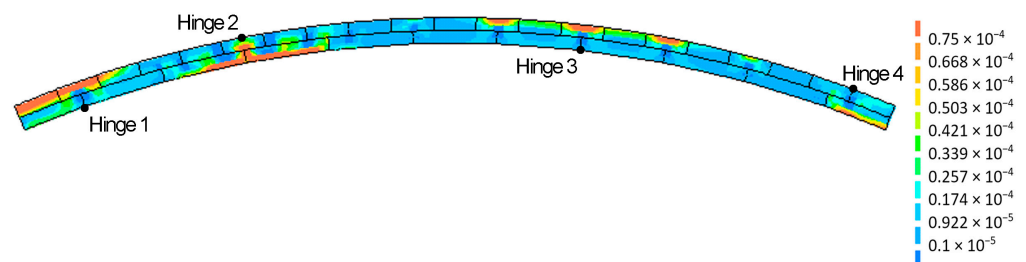
Figure 19. Principal tensile strains and hinges in the simplified micro-model.

3.4. Comparison of Results

Although the ultimate load capacity of both models is similar (14.35 and 14.25 kN for the macro- and micro-models, respectively), the numerical models based on the macro-modelling and simplified micro-modelling approaches present different deformations, namely, at the point placed at the opposite side of the loading point (Figure 20). The numerical models cannot match exactly with the experimental results, as the tested vaults presented different responses. Thus, an approximation of the numerical response to both experimental responses was expected, namely, a numerical response between both experimental results in terms of maximum load capacity and displacement. In what concerns damage, namely the collapse mechanism, the simplified micro-model allows for a more accurate identification of the hinges' position through the principal tensile strains, as the model itself is defined with more detail. On the other hand, the hinges in the macro-model appear as a diffuse stain distribution (Figures 15 and 19).

Figure 20. Load-displacement curves of the macro-model and the simplified micro-model: (**left**) response at the load point; and (**right**) response at the opposite side point.

4. Conclusions

This paper focuses on the structural analysis of tile vaults, aiming to enhance understanding of their behaviour and determine the most suitable approaches for their analysis. The complex structural characteristics of masonry pose challenges in accurate modelling. This research contributes to the ongoing discussion in academic and professional circles regarding the assessment methods for tile vaults.

A study on the structural performance of tile vaults is presented, involving experimental tests on masonry samples and two vaults, and graphical and numerical analysis. Limit analysis and non-linear static analysis were carried out. Two FEM models based on the macro-modelling and simplified micro-modelling approaches were prepared.

The two masonry full-scale structures showed brittle behaviour and presented the typical collapse mechanism with four hinges caused by a punctual load applied at $\frac{1}{4}$ of the vault's length. The ultimate loads were 16.0 kN and 13.19 kN for the first and the second vault, respectively.

The collapse load obtained from the limit analysis (3.84 kN) is significantly lower than the load capacity obtained from experimental tests (average of 14.59 kN). Although in general limit analysis is considered a reliable tool for the assessment of the structural behaviour of masonry structures, it was not able to predict correctly the load capacity of the tested tile vaults. The differences in the results can be related to one of the three well-known Heyman's assumptions for the application of the plastic theorems to masonry structures: masonry's tensile strength is considered null [44]. In light of the findings from the limit analysis, it would be highly beneficial to explore the integration of the tile vault's tensile capacity into this method. This inclusion would enable the application of the well-established and straightforward assessment method to tile vaults as well.

After the calibration process, the non-linear static analysis of both FEM models (macro-modelling and simplified micro-modelling approach) presented good results, mainly in terms of maximum load capacity (14 kN). Although the micro-model seems more appropriate to identify the position of the hinges, the macro-model presented better results in terms of deformation. Both FEM models were able to correctly replicate the damage observed in the experimental tests. Finally, it should be taken into account that the complexity in the preparation of the model (mesh and material properties) and the time needed for running the analyses for the micro-model are significantly higher than for the macro-modelling approach.

The comparative analysis of assessment methods for tile vaults enhances the understanding of their structural behaviour. By evaluating various approaches and elucidating their strengths and weaknesses, researchers and professionals are empowered to select the most suitable method for their specific needs. This research contributes to advancing the field of tile vault analysis and promotes the adoption of reliable assessment techniques. Embracing these advancements unlocks the potential of tile vaults in sustainable and efficient construction practices, enabling the creation of visually striking architectural designs with robust structural integrity. Through a comprehensive investigation of traditional construction techniques and their adaptation to contemporary standards, a paradigm shift toward a greener, more ecologically responsible future for construction is envisioned—one that embraces heritage while fostering innovative solutions for a planet in need.

References

1. Truñó, Á. *Construcción de Bóvedas Tabicadas*; The Library of the Col·legi d'Arquitectes de Catalunya: Barcelona, Spain, 1951.
2. Bergós, J. *Tabicados Huecos: Bases Para Las Dimensiones de Las Bóvedas y Cubiertas Del Templo Expiatorio de La Sagrada Familia*; Col·legi d'Arquitectes de Catalunya i Balears: Barcelona, Spain, 1965.
3. Choisy, A. *Histoire de l'architecture, Tome Premier*; Éditions Vincent, Fréal & Cie (Ed. 1955): Paris, France, 1899.
4. Collins, G.R. The Transfer of Thin Masonry Vaulting from Spain to America. *J. Soc. Archit. Hist.* **1968**, *27*, 176–201. [CrossRef]
5. Araguas, P. Voûte à La Roussillon. *Butlletí R. Acadèmia Catalana Belles Arts St. Jordi* **1999**, *13*, 173–185.
6. Fortea, M. Origen de La Bóveda Tabicada. In Proceedings of the Sexto Congreso Nacional de Historia de la Construcción, Valencia, Spain, 21–24 October 2009; Instituto Juan de Herrera: Madrid, Spain, 2009; pp. 491–500.
7. González Moreno-Navarro, J.L. La Bóveda Tabicada: Pasado y Futuro de Un Elemento de Gran Valor Patrimonial. In *Truñó, A. Construcción de Bóvedas Tabicadas*; Instituto Juan de Herrera: Madrid, Spain, 2004; pp. 11–60.
8. Ochsendorf, J. *Guastavino Vaulting: The Art of Structural Tile*; Reprint edition; Princeton Architectural Press: New York, NY, USA, 2013; ISBN 978-1-61689-244-9.
9. Douglas, I.; Napolitano, R.; Garlock, M.; Glisic, B. Reconsidering the Vaulted Forms of Cuba's National School of Ballet. In *Structural Analysis of Historical Constructions*; Aguilar, R., Torrealva, D., Moreira, S., Pando, M.A., Ramos, L.F., Eds.; Springer International Publishing: Cham, Switzerland, 2019; pp. 2150–2158.
10. Douglas, I.; Napolitano, R.K.; Garlock, M.; Glisic, B. Cuba's National School of Ballet: Redefining a Structural Icon. *Eng. Struct.* **2020**, *204*, 110040. [CrossRef]
11. Al Asali, M.W.; Couret, D.G.; Ramage, M.H. Beyond the National Art Schools: Thin-Tile Vaulting in Cuba after the Revolution. *J. Soc. Archit. Hist.* **2021**, *80*, 321–345. [CrossRef]
12. Del Curto, D.; Celli, S. The Treachery of Images: Redefining the Structural System of Havana's National Art Schools. *Sustainability* **2021**, *13*, 3767. [CrossRef]
13. Hughes, M.; Celli, S.; Heubner, C.; Garlock, M.; Ottoni, F.; Del Curto, D.; Wang, S.; Glisić, B. Nonlinear Finite-Element Analysis for Structural Investigation and Preservation of Reinforced Hybrid Thin Tile–Concrete Domes of the Historic School of Ballet Classrooms in Havana, Cuba. *J. Perform. Constr. Facil.* **2023**, *37*, 04022074. [CrossRef]
14. Block, P.; Van Mele, T.; Rippmann, M.; Ranaudo, F.; Calvo Barentin, C.; Paulson, N. Redefining Structural Art: Strategies, Necessities and Opportunities. *Struct. Eng.* **2020**, *98*, 66–72. [CrossRef]
15. De Wolf, C.; Ramage, M.; Ochsendorf, J. Low Carbon Vaulted Masonry Structures. *J. Int. Assoc. Shell Spat. Struct.* **2016**, *57*, 275–284. [CrossRef]
16. Leo Samuel, D.G.; Dharmasastha, K.; Shiva Nagendra, S.M.; Maiya, M.P. Thermal Comfort in Traditional Buildings Composed of Local and Modern Construction Materials. *Int. J. Sustain. Built Environ.* **2017**, *6*, 463–475. [CrossRef]

17. Nguyen, A.T.; Truong, N.S.H.; Rockwood, D.; Tran Le, A.D. Studies on Sustainable Features of Vernacular Architecture in Different Regions across the World: A Comprehensive Synthesis and Evaluation. *Front. Archit. Res.* **2019**, *8*, 535–548. [CrossRef]

18. Mumtaz, K.K.; Ahmed, H. The Shrine of Baba Hassan Din, Lahore. *J. Tradit. Build. Archit. Urban.* **2022**, *3*, 30–45. [CrossRef]

19. Rashid, M.; Ara, D.R. Modernity in Tradition: Reflections on Building Design and Technology in the Asian Vernacular. *Front. Archit. Res.* **2015**, *4*, 46–55. [CrossRef]

20. Özdeniz, M.B.; Bekleyen, A.; Gönül, I.A.; Gönül, H.; Sarigül, H.; Ilter, T.; Dalkiliç, N.; Yildirim, M. Vernacular Domed Houses of Harran, Turkey. *Habitat Int.* **1998**, *22*, 477–485. [CrossRef]

21. Keskin, K.; Erbay, M. A Study on the Sustainable Architectural Characteristics of Traditional Anatolian Houses and Current Building Design Precepts. *Procedia Soc. Behav. Sci.* **2016**, *216*, 810–817. [CrossRef]

22. Karabag, N.E.; Fellahi, N. Learning from Casbah of Algiers for More Sustainable Environment. *Energy Procedia* **2017**, *133*, 95–108. [CrossRef]

23. Dayaratne, R. Toward Sustainable Development: Lessons from Vernacular Settlements of Sri Lanka. *Front. Archit. Res.* **2018**, *7*, 334–346. [CrossRef]

24. Barbero-Barrera, M.M.; Gil-Crespo, I.J.; Maldonado-Ramos, L. Historical Development and Environment Adaptation of the Traditional Cave-Dwellings in Tajuña's Valley, Madrid, Spain. *Build. Environ.* **2014**, *82*, 536–545. [CrossRef]

25. Almssad, A.; Almusaed, A. Environmental Reply to Vernacular Habitat Conformation from a Vast Areas of Scandinavia. *Renew. Sustain. Energy Rev.* **2015**, *48*, 825–834. [CrossRef]

26. López López, D. *The Formwork as a Major Challenge in the Fabrication of Efficient, Economical and Sustainable Concrete Slabs. Blog of the Chair of Concrete Structures and Bridge Design, IBK, ETH Zurich*; ETH Zürich: Zürich, Switzerland, 2022.

27. López López, D.; Van Mele, T.; Block, P. Tile vaulting in the 21st century. *Inf. Construcción* **2016**, *68*, e162. [CrossRef]

28. Davis, L.; Rippmann, M.; Pawlofsky, T.; Block, P. Innovative funicular tile vaulting: A prototype vault in Switzerland. *Struct. Eng.* **2012**, *90*, 46–56.

29. López López, D.; Domènech Rodríguez, M.; Palumbo Fernández, M. "Brick-Topia", the Thin-Tile Vaulted Pavilion. *Case Stud. Struct. Eng.* **2014**, *2*, 33–40. [CrossRef]

30. Ramage, M.; Hall, T.J.; Gatóo, A.; Al Asali, M.W. Rwanda Cricket Stadium: Seismically Stabilised Tile Vaults. *Structures* **2019**, *18*, 2–9. [CrossRef]

31. Ramage, M.H.; Gatóo, A.; Al Asali, M.W. Complex Simplicity—Design of Innovative Sustainable Thin-Shell Masonry Structures. In *From Corbel Arches to Double Curvature Vaults: Analysis, Conservation and Restoration of Architectural Heritage Masonry Structures*; Milani, G., Sarhosis, V., Eds.; Research for Development; Springer International Publishing: Cham, Switzerland, 2022; pp. 257–281. ISBN 978-3-031-12873-8.

32. López López, D.; Van Mele, T.; Block, P. The Combination of Tile Vaults with Reinforcement and Concrete. *Int. J. Archit. Herit.* **2019**, *13*, 782–798. [CrossRef]

33. Dejong, M.; Ramage, M.; Travers, B.; Terry, S. Testing and Analysis of Geogrid-Reinforced Thin-Shell Masonry. In Proceedings of the 35th Annual Symposium of IABSE/52nd Annual Symposium of IASS/6th International Conference on Space Structures, London, UK, 20–23 September 2011.

34. Ramage, M.; Dejong, M. Design and Construction of Geogrid-Reinforced Thin-Shell Masonry. In Proceedings of the 35th Annual Symposium of IABSE/52nd Annual Symposium of IASS/6th International Conference on Space Structures, London, UK, 20–23 September 2011.

35. López López, D.; Bernat-Maso, E.; Gil, L.; Roca, P. Experimental Testing of a Composite Structural System Using Tile Vaults as Integrated Formwork for Reinforced Concrete. *Constr. Build. Mater.* **2021**, *300*, 123974. [CrossRef]

36. López López, D.; Roca, P.; Liew, A.; Van Mele, T.; Block, P. Tile Vaults as Integrated Formwork for Reinforced Concrete: Construction, Experimental Testing and a Method for the Design and Analysis of Two-Dimensional Structures. *Eng. Struct.* **2019**, *188*, 233–248. [CrossRef]

37. López López, D.; Bernat-Maso, E.; Saloustros, S.; Gil, L.; Roca, P. Experimental Testing and Structural Analysis of Composite Tile—Reinforced Concrete Domes. *Eng. Struct.* **2023**, *292*, 116512. [CrossRef]

38. Ramage, M.H.; Hall, T.; Rich, P. Light Earth Designs: Natural Material, Natural Structure. In *Earthen Architecture: Past, Present and Future*; CRC Press: Boca Raton, FL, USA, 2014; ISBN 978-0-429-22678-6.

39. Bertolesi, E.; Torres, B.; Adam, J.M.; Calderón, P.A.; Moragues, J.J. Effectiveness of Textile Reinforced Mortar (TRM) Materials for the Repair of Full-Scale Timbrel Masonry Cross Vaults. *Eng. Struct.* **2020**, *220*, 110978. [CrossRef]

40. Bertolesi, E.; Milani, G.; Adam, J.M.; Calderón, P.A. 3D Advanced Numerical Modelling of a Catalan-Layered Masonry Vault Unreinforced and Reinforced with Glass-TRM Materials and Subjected to Vertical Support Movements. In Proceedings of the 8th ECCOMAS Thematic Conference on Computational Methods in Structural Dynamics and Earthquake Engineering, Athens, Greece, 28–30 June 2021; pp. 415–422.

41. Castori, G.; Borri, A.; Corradi, M. Behavior of Thin Masonry Arches Repaired Using Composite Materials. *Compos. Part B Eng.* **2016**, *87*, 311–321. [CrossRef]

42. Corradi, M.; Castori, G.; Borri, A. A New Method for Strengthening Tiled Vaults: "Reinforced Catalan Vaulting". In Proceedings of the 9th International Masonry Conference, Guimarães, Portugal, 7–9 July 2014.

43. Savino, V.; Franciosi, M.; Viviani, M. Engineering and Analyses of a Novel Catalan Vault. *Eng. Fail. Anal.* **2023**, *143*, 106841. [CrossRef]

44. Heyman, J. The Stone Skeleton. *Int. J. Solids Struct.* **1966**, *2*, 249–279. [CrossRef]

45. Andreu, A.; Gil, L.; Roca, P. Computational Analysis of Masonry Structures with a Funicular Model. *J. Eng. Mech.* **2007**, *133*, 473–480. [CrossRef]

46. Block, P.; Lachauer, L. Three-Dimensional (3D) Equilibrium Analysis of Gothic Masonry Vaults. *Int. J. Archit. Herit.* **2014**, *8*, 312–335. [CrossRef]

47. Block, P.; Ciblac, T.; Ochsendorf, J. Real-Time Limit Analysis of Vaulted Masonry Buildings. *Comput. Struct.* **2006**, *84*, 1841–1852. [CrossRef]

48. Fraternali, F. A Thrust Network Approach to the Equilibrium Problem of Unreinforced Masonry Vaults via Polyhedral Stress Functions. *Mech. Res. Commun.* **2010**, *37*, 198–204. [CrossRef]

49. Bertolesi, E.; Milani, G.; Carozzi, F.G.; Poggi, C. Ancient Masonry Arches and Vaults Strengthened with TRM, SRG and FRP Composites: Numerical Analyses. *Compos. Struct.* **2018**, *187*, 385–402. [CrossRef]

50. Alexakis, H.; Makris, N. Hinging Mechanisms of Masonry Single-Nave Barrel Vaults Subjected to Lateral and Gravity Loads. *J. Struct. Eng.* **2017**, *143*, 04017026. [CrossRef]

51. Chiozzi, A.; Milani, G.; Grillanda, N.; Tralli, A. A Fast and General Upper-Bound Limit Analysis Approach for out-of-Plane Loaded Masonry Walls. *Meccanica* **2018**, *53*, 1875–1898. [CrossRef]

52. Chiozzi, A.; Milani, G.; Tralli, A. A Genetic Algorithm NURBS-Based New Approach for Fast Kinematic Limit Analysis of Masonry Vaults. *Comput. Struct.* **2017**, *182*, 187–204. [CrossRef]

53. Chiozzi, A.; Milani, G.; Tralli, A. Fast Kinematic Limit Analysis of FRP-Reinforced Masonry Vaults. I: General Genetic Algorithm–NURBS–Based Formulation. *J. Eng. Mech.* **2017**, *143*, 04017071. [CrossRef]

54. Milani, G. Upper Bound Sequential Linear Programming Mesh Adaptation Scheme for Collapse Analysis of Masonry Vaults. *Adv. Eng. Softw.* **2015**, *79*, 91–110. [CrossRef]

55. Dinani, A.T.; Destro Bisol, G.; Ortega, J.; Lourenço, P.B. Structural Performance of the Esfahan Shah Mosque. *J. Struct. Eng.* **2021**, *147*, 05021006. [CrossRef]

56. Saloustros, S.; Pelà, L.; Roca, P.; Portal, J. Numerical Analysis of Structural Damage in the Church of the Poblet Monastery. *Eng. Fail. Anal.* **2015**, *48*, 41–61. [CrossRef]

57. Creazza, G.; Matteazzi, R.; Saetta, A.; Vitaliani, R. Analyses of Masonry Vaults: A Macro Approach Based on Three-Dimensional Damage Model. *J. Struct. Eng.* **2002**, *128*, 646–654. [CrossRef]

58. Oñate, E.; Hanganu, A.; Barbat, A.; Oller, S.; Vitaliani, R.; Saetta, A.; Scotta, R. Structural Analysis and Durability Assesment of Historical Constructions Using a Finite Element Damage Model. In *Structural Analysis of Historic Construction: Possibilities of Numerical and Experimental Techniques*; CIMNE: Barcelona, Spain, 1995; pp. 189–224.

59. Atamturktur, S.; Sevim, B. Seismic Performance Assessment of Masonry Tile Domes through Nonlinear Finite-Element Analysis. *J. Perform. Constr. Facil.* **2012**, *26*, 410–423. [CrossRef]

60. Pantò, B.; Cannizzaro, F.; Caddemi, S.; Caliò, I.; Chácara, C.; Lourenço, P.B. Nonlinear Modelling of Curved Masonry Structures after Seismic Retrofit through FRP Reinforcing. *Buildings* **2017**, *7*, 79. [CrossRef]

61. D'Altri, A.M.; De Miranda, S.; Castellazzi, G.; Sarhosis, V.; Hudson, J.; Theodossopoulos, D. Historic Barrel Vaults Undergoing Differential Settlements. *Int. J. Archit. Herit.* **2020**, *14*, 1196–1209. [CrossRef]

62. Bianchini, N.; Mendes, N.; Calderini, C.; Lourenço, P.B. Modelling of the Dynamic Response of a Reduced Scale Dry Joints Groin Vault. *J. Build. Eng.* **2023**, *66*, 105826. [CrossRef]

63. Milani, G.; Rossi, M.; Calderini, C.; Lagomarsino, S. Tilting Plane Tests on a Small-Scale Masonry Cross Vault: Experimental Results and Numerical Simulations through a Heterogeneous Approach. *Eng. Struct.* **2016**, *123*, 300–312. [CrossRef]

64. Roca, P.; Cervera, M.; Gariup, G.; Pela', L. Structural Analysis of Masonry Historical Constructions. Classical and Advanced Approaches. *Arch. Comput. Methods Eng.* **2010**, *17*, 299–325. [CrossRef]

65. López López, D.; Domènech Rodríguez, M. *Tile Vaults: Structural Analysis and Experimentation. 2015 Guastavino Biennial*; Ajuntament de Barcelona: Barcelona, Spain, 2017.

66. Rots, J.G. *Structural Masonry: An Experimental/Numerical Basis for Practical Design Rules (CUR Report 171)*; Balkerma: Rotterdam, The Netherlands, 1977.

67. Lourenço, P.B. Computational Strategies for Masonry Structures. Ph.D. Thesis, Delft University of Technology, Delft, The Netherlands, 1996.

68. Placo Saint-Gobain. Available online: https://www.placo.es/ (accessed on 9 June 2023).

69. *UNE-EN 13.279-1:2006*; Yesos de Construcción y Conglomerantes a Base de Yeso Para la Construcción. AENOR: Madrid, Spain, 2006.

70. Comite Euro-International Du Beton. *CEB-FIP Model Code 1990: Design Code*; Thomas Telford Services Ltd.: Lausanne, Switzerland, 1993.

71. Lourenço, P.B. Recent Advances in Masonry Modelling: Micromodelling and Homogenisation. In *Multiscale Modeling in Solid Mechanics*; Computational and Experimental Methods in Structures; Imperial College Press: London, UK, 2009; Volume 3, pp. 251–294, ISBN 978-1-84816-307-2.

72. *EN 1015-11*; Methods of Test for Mortar for Masonry. European Committee for Standardization: Brussels, Belgium, 2000.

73. Lourenço, P.B. Computations on Historic Masonry Structures. *Prog. Struct. Eng. Mater.* **2002**, *4*, 301–319. [CrossRef]

74. Mendes, N. Masonry Macro-Block Analysis. In *Encyclopedia of Earthquake Engineering*; Beer, M., Kougioumtzoglou, I.A., Patelli, E., Au, I.S.-K., Eds.; Springer: Berlin/Heidelberg, Germany, 2014; pp. 1–10. ISBN 978-3-642-36197-5.

75. López López, D.; Roca, P.; Liew, A.; Méndez Echenagucia, T.; Van Mele, T.; Block, P. A Three-Dimensional Approach to the Extended Limit Analysis of Reinforced Masonry. *Structures* **2022**, *35*, 1062–1077. [CrossRef]
76. DIANA FEA. *User's Manual—Release 10.2 2017*; DIANA FEA: Delft, The Netherlands, 2017.